Enhanced high-pressure superconductivity and local structure of the Ba8 Si46 clathrate

F. Morales, M. Núñez-Regueiro, Pierre Toulemonde, D. Machon, S. Le Floch, V. Pischedda, P. Lagarde, A. Flank, J. Itié, A. San-Miguel

Enhanced high-pressure superconductivity and local structure of the Ba_8Si_{46} clathrate

F. Morales,[1] M. Núñez-Regueiro,[2,3] P. Toulemonde,[2,3] D. Machon,[4,5] S. Le Floch,[4,5] V. Pischedda,[4,5] P. Lagarde,[6] A.-M. Flank,[6] J. P. Itié,[6] and A. San-Miguel[4,5]

[1]*Instituto de Investigaciones en Materiales, Universidad Nacional Autónoma de México, México, D.F. 04510, México*

[2]*CNRS, Institut Néel, F-38000 Grenoble, France*

[3]*Université Grenoble Alpes, Institut Néel, F-38000 Grenoble, France*

[4]*Université de Lyon, F-69000 Lyon, France*

[5]*Institut Lumière Matière, CNRS, UMR 5306, Université Lyon 1, F-69622 Villeurbanne, France*

[6]*Synchrotron SOLEIL, L'Orme des Merisiers Saint-Aubin, BP 48, 91192 Gif sur Yvette Cedex, France*

(Received 14 June 2016; revised manuscript received 23 August 2016; published 13 September 2016)

The high-pressure superconducting properties and the local structure of the Ba_8Si_{46} clathrate have been studied using electrical resistance and x-ray absorption spectroscopy measurements up to more than 20 GPa. At pressures above 10–13 GPa, corresponding to a well-known volume collapse phase transformation, a sudden increase in the critical temperature leads to a maximum value of the superconducting critical temperature T_c of ∼8.5–9 K at 20 GPa. In the low-pressure clathrate phase, the superconducting critical temperature decreases as pressure is applied with an electron-phonon coupling constant $\lambda = 1.1$ derived from the temperature evolution of the electrical resistance at different pressures. A progressive disorder in the Ba-Si correlations in the $Ba@Si_{24}$ cages of the structure is observed for pressures beyond ∼5 GPa. These observations exclude a structural homothecy at the volume collapse transition. The high-pressure collapsed phase of Ba_8Si_{46} is then associated with local structural changes and shows enhanced superconducting properties.

DOI: 10.1103/PhysRevB.94.104507

I. INTRODUCTION

Group-IV clathrate compounds are nanocage sp^3-based structures allowing for endohedral guest atom intercalation. They attract high interest due to their superconductivity [1,2], as potential ultrahard materials [3,4], or as a prototype for ternary compounds currently investigated for thermoelectrical properties [5–7]. In the clathrate structures the host lattice-phonon structure is highly decoupled from the guest lattice which from its side can provide the charge carriers. Such type of structural arrangement appears to strongly favor superconductivity as has been shown not only in silicon clathrates [8] but also in recent calculations on hydride clathrate structures such as CaH_6 [9] or YH_6 [10] with predictions of high-pressure superconducting critical temperatures beyond 260 K. Understanding how superconductivity properties evolve in clathrate structures at high pressures appears then as an important ingredient in the quest of higher critical temperature superconductors. Silicon clathrates crystallize in different structures which are differentiated into types, of which type-I and type-II are the most studied [11,12]. The type-I compounds can be viewed as composed of two Si_{20} and six Si_{24} nanocages per unit cell, while the type-II are composed by eight Si_{20} and sixteen Si_{28} nanocages [13]. Other clathrate related structures of type I exist [14,15]. In all these clathrate structures the Si atoms are interlinked through tetrahedral sp^3 covalent bonds leading to nanocages assembled through sharing faces. These cagelike compounds have an adequate topology for hosting other elements. In particular, silicon clathrates hosting alkaline or earth-alkaline elements in all the nanocages form compounds with ideal formula M_8Si_{46} for the type-I clathrates and $M_{24}Si_{136}$ for the type-II compounds, where M is the guest element. The presence of guest atoms modifies the electronic properties. For example, Na and Ba hosting in type-I clathrates leads to superconductivity below 4 K [1]. When only Ba is intercalated the superconducting critical temperature increases to about 8 K [16] having a BCS character with multigap signatures [17–19]. Superconductivity has also been measured with lower critical temperatures in $(Ba_{1-x}Sr_x)_8Si_{46}$ [20] or in the type-III clathrate $Ba_{24}Si_{100}$ [21]. It is noteworthy that silicon is not a superconducting material under normal conditions in its diamond tetrahedral sp^3 structure, but it transits to a superconducting state when subjected to high pressure [22] as well as through high boron doping [23]. Silicon in the β-Sn structure, i.e., above 11.5 GPa, is superconducting with $T_c \simeq 6.3$ K at 12 GPa. At pressures above 14 GPa there is a new structural transition from the β-Sn phase to a simple hexagonal phase; this transition occurs at room temperature. At low temperatures, silicon in the simple hexagonal structure is superconducting at pressures above 13.5 GPa, reaching its highest T_c of 8.2 K under a pressure of 15.2 GPa [22].

The high-pressure structural evolution of silicon clathrates is strongly influenced by the nature of the guest atoms. The Na-filled type-I silicon clathrate under high pressure decomposes from 14 GPa and the hexagonal phase of silicon is observed [3,24]. The situation is totally different for heavier guest atoms [25] as in Ba_8Si_{46} [24,26–30], K_8Si_{46} [31,32], $I_8Si_{44}I_2$, or Rb_8Si_{46} [33]. Their high-pressure evolution is first characterized by the preservation of the tetrahedral silicon clathrate structure for pressures up to more than 4 times the stability domain of the diamond phase and, second, by a progressive volume collapse in a rather narrow pressure domain [25]. In Ba_8Si_{46} the collapse transition is observed at 14–16 GPa [24]. A first transition at about 5–7 GPa precedes this one as evidenced by crystallographic structural measurements by x-ray diffraction and x-ray absorption spectroscopy [27] as well as Raman spectroscopy [26]. This transition has been discussed as due to displacements of the Ba atoms within the Si_{24} cages [28] preserving the host-atom type-I clathrate structure. The second transition at about 15 GPa has been first described as a homothetic volume collapse

[24,27] and is also observed in type-III silicon clathrates [34]. To explain this second transition other mechanisms have been proposed as an electron topological transition related to an extensive rehybridization of the Si atoms leading to a transfer of valence electrons from the bonding to the interstitial region inside the cages [30]. Finally, the diffusion of some of the silicon atoms in the (6*c*) Wyckoff positions of the cages [35] has been proposed to explain the lower bulk modulus of the high-pressure phase. Whatever the case, the importance of the role of the (6*c*) Si positions seems to be confirmed by the high-pressure Raman spectroscopy comparison of different chemical substituted compounds based on Ba_8Si_{46} [36].

Superconducting transition temperatures, as a function of pressure, have been reported in Ba_8Si_{46} by resistance versus temperature measurements up to 1.8 GPa [8]. In this pressure range T_c decreases as the pressure increases, going from a T_c of 8 K at ambient pressure to $\simeq$6.8 K at 1.8 GPa. In another study [30] the electrical resistance of Ba_8Si_{46} was measured up to pressures of 20 GPa but in a temperature domain between 80 and 280 K which did not allow exploring the superconducting properties.

In this work we have studied both the pressure evolution of the electronic transport properties at low temperatures of the Ba_8Si_{46} clathrate and the evolution of the local structure of its guest atoms (Ba) up to pressures beyond 20 GPa, i.e., beyond the volume collapse pressure. The superconducting critical temperature T_c decreases as the pressure increases up to 14 GPa reaching a $T_c \sim 3$ K; however, at higher pressures T_c increases reaching $T_c \sim 8.5$–9 K at 20 GPa, showing that the high-pressure collapsed phase is also superconducting. The local structure studied by XAS shows a clear evolution from 5 GPa. The correlation between the two studies allows one to obtain better insight on the electron-phonon coupling mechanism driving the superconducting properties of Si clathrates, to discuss the possible role of Ba substoichiometry on the first high-pressure transition at 5–7 GPa, and to restrict the scenario on the nature of the collapse transition.

II. EXPERIMENTAL

Ba_8Si_{46} powder samples were prepared following the high-pressure route in a belt apparatus following Refs. [25,37]. Starting from the $BaSi_2$ Zintl phase mixed with silicon powder and placed in an h-BN cell, the synthesis occurs at 1000 K under high pressure (1–5 GPa). The sample is quenched at room temperature before the pressure is slowly released. The powder samples were finely ground to obtain homogeneous powders.

The high-pressure electrical resistivity measurements were performed in a sintered diamond Bridgman anvil apparatus using a pyrophyllite gasket and two steatite disks as the pressure medium. The Cu-Be device that locked the anvils can be temperature cycled between 1.2 K and 300 K inside a sealed Dewar. Pressure was calibrated against the various phase transitions of Bi under pressure at room temperature, and with a superconducting Pb manometer at lower temperatures. The overall uncertainty in the quasihydrostatic pressure is estimated to be $\pm$15%. The pressure spread across the sintered diamond anvils was previously determined on Pb manometers within 1.5–2 GPa depending on the applied pressure. The temperature was determined using a calibrated

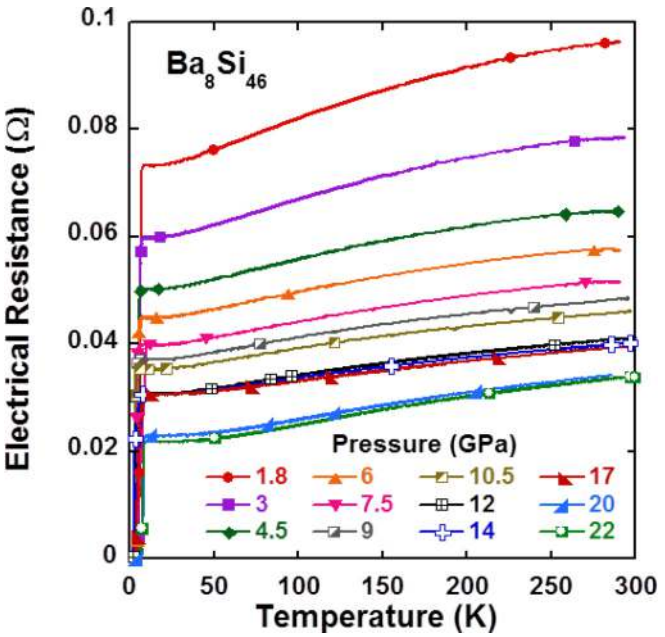

FIG. 1. Electrical resistance as function of temperature at different pressures in Ba_8Si_{46}. Symbols do not denote measured points but just serve to identify curves.

Cernox thermometer with a maximum uncertainty (due mainly to temperature gradients across the Cu-Be clamp) of 0.5 K. Four-probe electrical resistivity dc measurements were carried out through platinum wires in contact with the sample, using a Keithley 182 nanovoltmeter combined with a Keithley 238 current source. Two samples, of the same batch, were measured giving similar behavior.

X-ray absorption experiments at the Ba L_{III} edge (5248 eV) and L_{II} edge (5624 eV) under high pressure were performed at the LUCIA beamline [38] at the SLS synchrotron source. The sample was loaded in a perforated double diamond anvil cell in order to reduce the x-ray absorption from the diamond anvils. Silicon oil was used as a pressure-transmitting medium and pressure was calibrated using the *in situ* ruby luminescence method [39]. Spectra were taken up to a maximum pressure of 20.5 GPa. X-ray absorption data were analyzed on the Ba L_{III} edge spectra by combining the extended x-ray absorption fine structure (EXAFS) data extraction using the CDXAS code [40] and the FEFF [41] and FEFFIT [42] ones for EXAFS fitting.

III. ELECTRICAL RESISTANCE UNDER HIGH PRESSURE

In Fig. 1 we show the temperature dependence of the electrical resistance of one sample as a function of pressure. The smooth variation of our curves contrasts with the measurements of Ref. [30]. This can be explained by the difficulties of the diamond anvil cell experiments and by the use in that work of MgO as a pressure-transmitting medium. In our case, the use of larger sample sizes and the use of a more hydrostatic pressure-transmitting medium (steatite) would explain the better data quality. At the lowest pressure the electrical resistance temperature dependence has an S shape characteristic of a bad but superconducting metal.

It also shows a very small residual resistance ratio (RRR) ∼1.3, defined as the ratio of resistance at room temperature to the extrapolated resistance at 0 K. This ratio gives a measure of the relevance of the electron scattering by impurities and defects. The small value for RRR implies a large number of defects, which may correspond to numerous ion vacancies due to barium substoichiometry. In fact, the nominal Ba_8Si_{46} clathrate is usually obtained in high-pressure synthesis in the substoichiometry form, $Ba_{8-x}Si_{46}$, with values $0.24 \leqslant x \leqslant 0.39$ [16] or even higher [43]. As a function of pressure, the resistance of our samples decreases monotonically, though more slowly for pressures larger than 10 GPa.

It is interesting to analyze the low-temperature dependence trying to determine the dominating carrier scattering above the superconducting transition. We have found that within the range of 20 to 40 K the dependence is clearly quadratic in temperature, as shown in Fig. 2(a), where we plot the low-temperature resistance as a function of the square of the temperature.

Quadratic temperature dependencies can be due to numerous reasons [44], and have been observed and thoroughly studied in superconductors [45]. Taking into account that we have a very strong impurity scattering, the most favorite candidate to explain the observed quadratic behavior is inelastic scattering against impurities [46] or Koshino-Taylor (K-T) scattering. If K-T scattering is the main reason for the quadratic temperature term, then the coefficient of the quadratic term should be directly proportional to the residual resistance [47], R_0 (RRR), with a slope around $\sim 10^{-5}$ K^{-2}. We show in Fig. 2(b) that this is indeed the case, with a slope of 2×10^{-5} K^{-2}. So, the impurities not only generate a strong elastic scattering, measured by the RRR, but also produce a strong inelastic scattering yielding an unusually large quadratic temperature term, A. Nevertheless, as T_c also scales with A, we can attempt the Fermi liquid fit [48], $T_c = \theta e^{-\zeta/\sqrt{A}}$, where θ and ζ are adjustable parameters, which allow us to estimate the electron-phonon coupling constant of Ba_8Si_{46}, $\lambda = \sqrt{A}/\zeta$. As the slope that we obtain for $A/R_0 = 2 \times 10^{-5}$, i.e., the double of the expected one [45], we have corrected the measured value of A, subtracting the K-T term, $A'(P) = A(P) - 10^{-5}R_0(P)$, and performed the fit with A'. Figure 3 shows the relation between T_c and the square root of A'. We obtain at ambient pressure $\lambda = 1.1$, in good agreement with the one calculated in Ref. [8], $\lambda = 1.05$. Our result shows that even if the K-T is present, it does not dominate all the T^2 scattering and a quite good estimate of the coupling parameter can be obtained by the Fermi liquid fit.

We now discuss the superconducting transition and its evolution with pressure, shown in Fig. 4. The superconducting transition temperature first decreases gradually and then, beyond ∼15 GPa, increases with pressure. Between 12 and 17 GPa, the transition seems double (there are two maxima in the temperature derivative of the resistance curve), as if there were a coexistence of two different phases. This coexistence region seemingly corresponds to the volume collapse transition observed in combined x-ray diffraction and x-ray absorption spectroscopy experiments [24,27,30].

The pressure dependence of the superconducting transition temperature is shown in Fig. 5(a). The decrease followed by the increase of T_c is clear, as it is also the existence of two

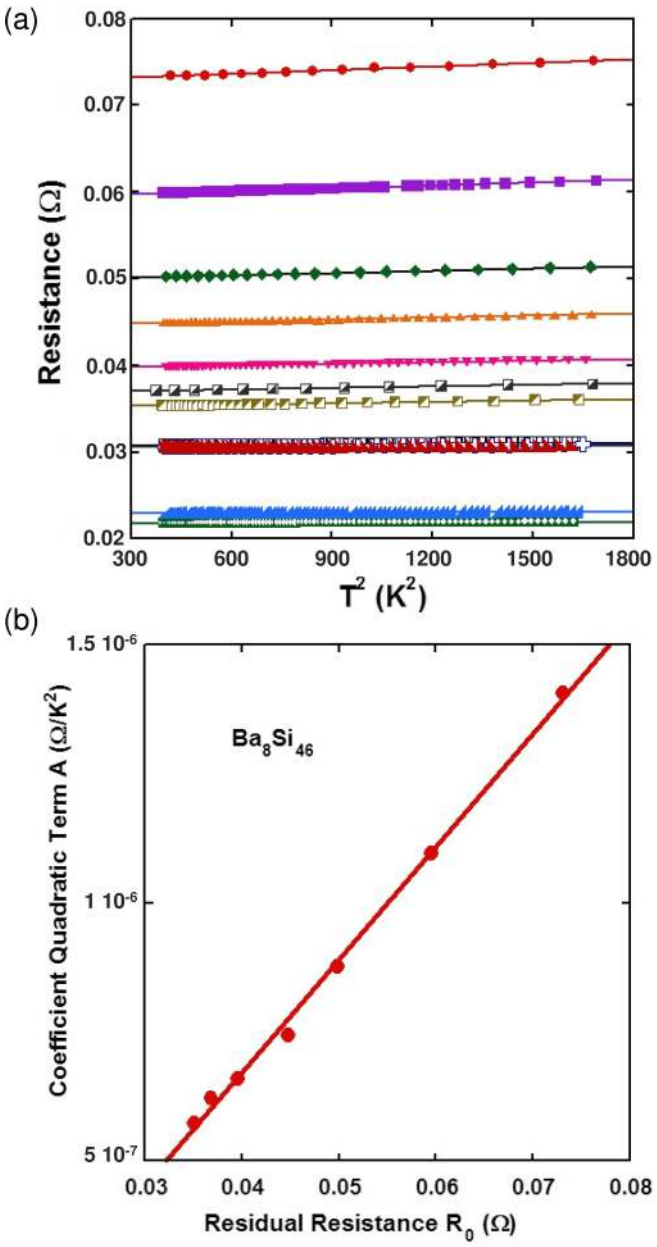

FIG. 2. (a) Low-temperature electrical resistances, within the range of 20 K to 40 K, of Ba_8Si_{46} as a function of the square of the temperature. It shows a defined dependence. Symbols are the same as those of Fig. 1. (b) Correlation between A, the coefficient of the quadratic temperature term, and the residual resistivity. It is clearly linear with a slope of 2.18×10^{-5} K^{-2}. It shows that this term is due to inelastic scattering of carriers against impurities.

different transition onsets in the coexistence region between the volume-collapsed and the noncollapsed phase. This is further evidenced in Fig. 5(b) by plotting the width of the transition zone taken as the temperature domain between the onset of the transition and the zero resistivity. We distinguish clearly three regimes, with the intermediate one between ∼12 and 17 GPa corresponding to a phase mixing.

The T_c pressure decrease was previously measured below 1.8 GPa and its pressure dependence calculated theoretically [8]. Our data for the low-pressure phase follow nicely the

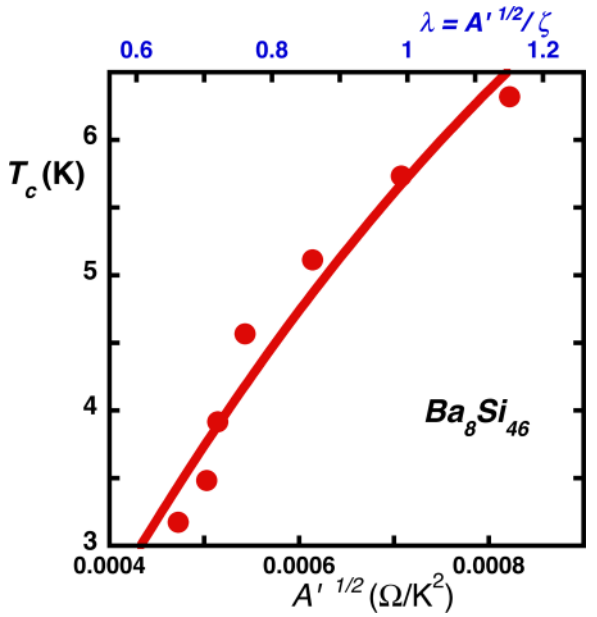

FIG. 3. Fermi liquid fit $T_c = \theta e^{-\zeta/\sqrt{A}}$ on the corrected coefficient $A'(P) = A(P) - 10^{-5}R_0$. We obtain an ambient pressure $\lambda = 1.1$, in very good agreement with the calculations of Ref. [8], which give $\lambda = 1.05$.

calculated dependence as shown by the dashed-point curve of Fig. 5(a). Thus, the behavior of superconductivity with pressure for the clathrate low-pressure phase seems well understood. However, the data for the high-pressure phase, i.e., above the volume collapse starting at 13–15 GPa, are more difficult to grasp. In the high-pressure phase, the higher T_c could be ascribed to an enhancement of the hybridization of the barium orbitals by volume reduction. This appears as

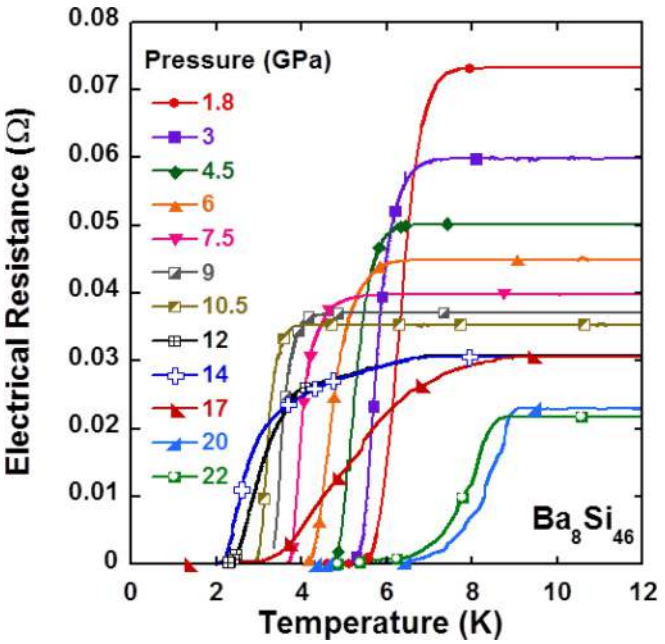

FIG. 4. Superconducting transition in Ba_8Si_{46} at high pressure. We observe a decrease of T_c with pressure, followed by an increase beyond 14 GPa.

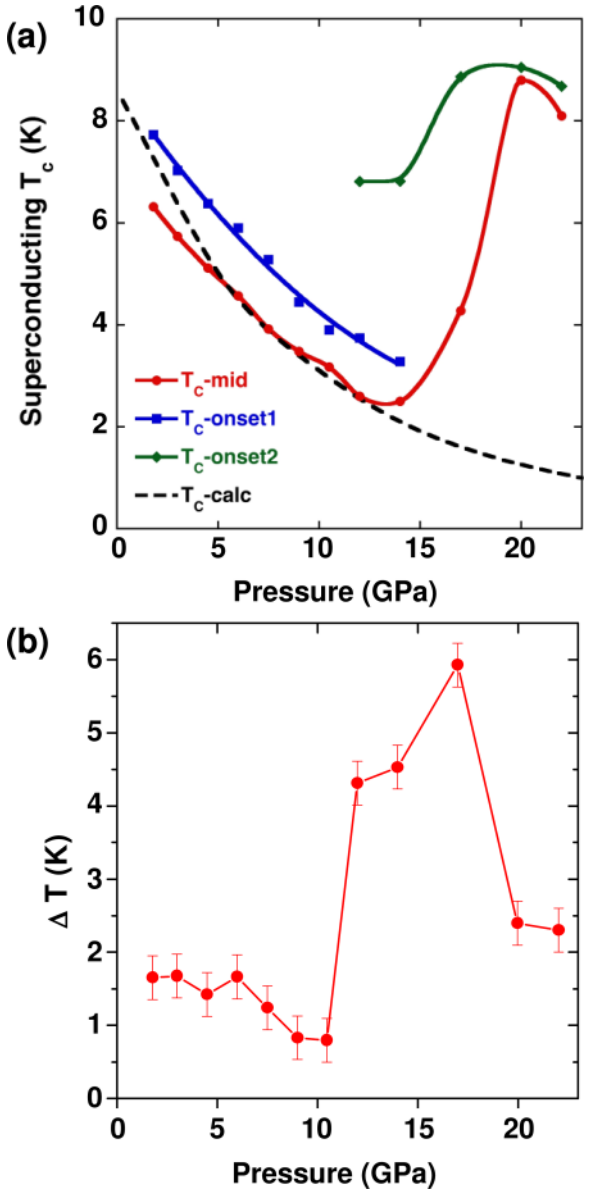

FIG. 5. (a) Dependence of the superconducting transition temperature, T_c, with pressure. We observe a decrease followed by an increase above 14 GPa. The decrease follows the previously calculated pressure dependence of T_c (dashed curve, from Ref. [8]). In the region of coexistence we can determine two different onsets, which seem to be associated with the two different phases. (b) Dependence of the temperature width of the superconducting transition as observed in Fig. 4. The line is a guide for the eye.

contradictory with the observed evolution in the low-pressure phase (before the volume collapse). This result, then, does not support the idea of a homothetic volume collapse but of a change of structure implying new schemes of hybridization as suggested in Refs. [29,35]. On the other hand, due to the proximity of the T_c values to the ones of the simple hexagonal high-pressure phase of silicon [22], we may be tempted to speculate that some portion of the clathrate sample may be dissociated and lead to microcrystalline silicon even if the T_c evolution with pressure for pure silicon does not correspond to the one measured here for $P > 13$ GPa.

In order to test that hypothesis, we cycled Ba_8Si_{46} up to 17 GPa using a Paris-Edinburgh press with sintered diamond anvils [49]. We did not use a pressure-transmitting medium to better mimic the experimental conditions in our electric transport measurements and compared the x-ray diffraction pattern before and after the pressure cycle. The diffraction pattern was clearly reversible and it was not possible to distinguish any trace of silicon in its diamond form within the experimental resolution of the diffractometer. There was no trace of presence of the characteristic diffraction peaks from other silicon metastable phases obtained after pressure cycling as BC8 [50]. The zero resistivity observed beyond 13–15 GPa would imply at least one third of the sample in the superconducting state. This clearly excludes the idea of a high-pressure segregation and supports the idea that the superconducting behavior at $P > 15$ GPa does correspond to the high-pressure phase of Ba_8Si_{46} with a modified structure.

We then use x-ray absorption spectroscopy as a complementary technique to x-ray diffraction or Raman spectroscopy to obtain insight on the high-pressure local effects [51] on the properties of Ba_8Si_{46}.

IV. X-RAY ABSORPTION SPECTROSCOPY

X-ray absorption spectroscopy allows us to extract local structural and electronic property information from selected atomic species in condensed matter systems [52,53]. Figure 6 shows the x-ray absorption near edge structure (XANES) evolution at the Ba L_{III} edge during compression. The Ba L_{II} edge XANES signal is shown in Fig. S1 of the Supplemental Material [54], but we will concentrate our discussion on the Ba L_{III} edge data which had a better signal to noise ratio. The here obtained data quality contrasts with the XANES data from Ref. [27] in which essentially only the edge position and the white line could be measured (in that work two XAS studies were included: one at the Ba L_{III} edge in energy dispersive mode up to 20 GPa and another at the Ba K edge in XAS scanning mode up to 14.4 GPa). Here we observe a clear modification of the XANES resonances for pressures beyond 13.0 GPa in correspondence with the collapse pressure domain in Ba_8Si_{46}. This change can be described in particular by an important modification of the intensity ratio of the two first XANES resonances after the white line (the first prominent XANES peak just after the absorption edge). Homothetic compression associated with the volume reduction could be in principle at the origin of intensity ratio modifications of XANES resonances [55]. Nevertheless, the stability of the two XANES profiles below and beyond 13.0 GPa (with similar volume changes in the two pressure domains) points to a clear evolution of the local structure at the volume collapse transition.

The pressure evolution of the absorption edge energy can provide information on the evolution of the symmetry-projected local electronic structure of the absorbing atoms. The obtained evolution is shown in Fig. S2 of the Supplemental Material [54] and compared with the already reported evolution in Ref. [27] using an energy-dispersive XAS optics [56]. Both data are in good agreement showing a down-shift of the edge position of about 0.5 eV at 3–5 GPa. The edge position remains then constant until the collapse transition where the Ba L_{III} position starts to decrease steadily at a rate of -60 meV GPa^{-1}. The onset of the collapse transition can be set between 10 and 13 GPa in the present experiment in good agreement with Ref. [27], where it was found to lie between 11.5 and 14 GPa.

The extracted EXAFS signal is shown in Fig. 7. The proximity of the L_{II} edge limits the maximum energy domain

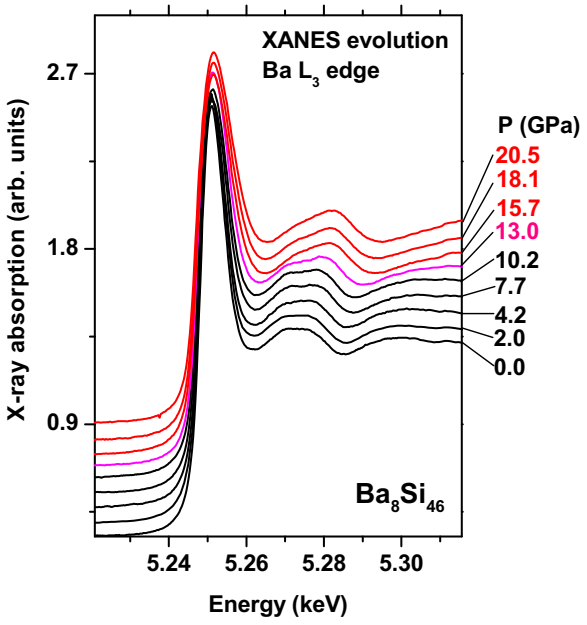

FIG. 6. Evolution of the Ba L_{III} XANES signal in Ba_8Si_{46} as a function of pressure. The spectra have been vertically shifted for clarity. Pressure is indicated at the right side. In red are the spectra corresponding to the collapsed phase.

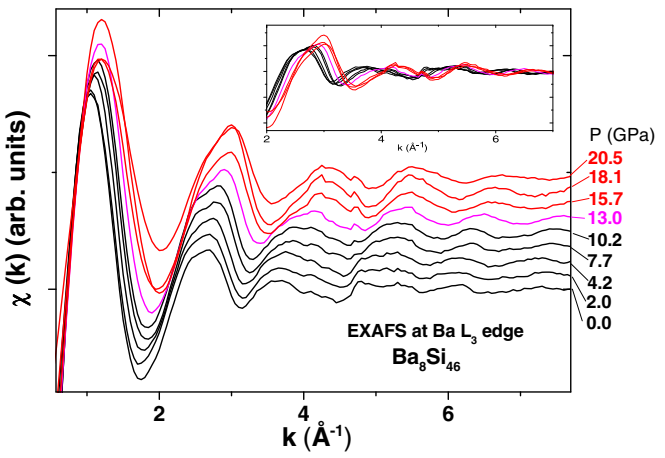

FIG. 7. Evolution of the Ba L_{III} EXAFS signal in Ba_8Si_{46} as a function of pressure. The spectra have been shifted vertically for clarity. The different colors correspond to the spectra before the collapse transition (black) and after the collapse transition (red). The spectrum at 13.0 in magenta is intermediate. In the inset the spectra have been superimposed allowing us to better distinguish the differences between the spectra before and after the collapse transition.

available after the L_{III} edge to 380 eV. In spite of this limitation, we observe a clear change in the oscillation scheme for pressures beyond 13.0 GPa. This change is rather strong and difficult to justify by the only volume reduction associated with the smooth volume collapse. Then, a modification in the local structure around the Ba atom after the pressure collapse appears as a clear plausible hypothesis in agreement with our XANES data and other studies [29]. We would like to underline that in previous works [27] EXAFS data were only obtained for pressures below the collapse pressure. Due to the limited k range allowed for the EXAFS fitting available in our experiment (Fig. 7), several fitting schemes were tested. All of them included the k-space fitting of the Fourier-transformed filtered signal within the type-I clathrate model using the *ab initio* calculation of the atomic scattering amplitude and phase shift for each scattering path using the FEFF code [41] and the fit within that structural model using FEFFIT [42].

In our fitting model, only the local cage environment around each Ba atom made of Si_{20} and Si_{24} cages was fitted. This was done by filtering the Fourier-transformed signal obtained from a k domain between 3 and 7 $Å^{-1}$ (see Fig. S3 of the Supplemental Material [54]). We observe clearly in the Fourier transform that the signal is dominated by a double peak at phase-shift-uncorrected distances below 3.2 Å, which correspond to the cage shell. The R-space filtered signal corresponding to that doublet was inverse Fourier transformed and fitted within the type-I clathrate model. Best fits were obtained by considering as input fitting parameters the high-pressure cell parameters obtained by x-ray diffraction [27] at each pressure point and only considering as free variables the pseudo-Debye temperatures associated to the Ba-Si scattering paths in each one of the two cages and the cell parameters themselves. The pseudo-Debye Waller factor is a measurement of the static (disorder) or dynamic (thermal agitation) loss of coherence projected in the EXAFS scattering paths [57], i.e., the Ba-Si distances in the cages in our case. It is frequent to use the associated Debye temperature of a pure dynamic and harmonic pseudo-Debye Waller to characterize it [57]. In the absence of static disorder the peudo-Debye temperature will then increase with pressure as a result of the bond strengthening in correspondence with the increase of the Debye temperature of the material. Figure 8 shows the obtained results for the pressure evolution of the relative pseudo-Debye temperature associated with the Ba-Si paths in the Si_{20} and Si_{24} cages. The obtained cell parameters in the compression cycle were in excellent agreement with the ones obtained by x-ray diffraction in previous works (see Fig. S4 of the Supplemental Material [54]). The relative evolution of the pseudo-Debye temperature associated with the Ba-Si scattering paths in the Si_{20} and Si_{24} cages shows a continuous but totally opposite evolution with pressure. This qualitative evolution is also well reproduced by the other EXAFS models which we tested in our work.

We were able to improve the fit quality for the three data points between 4.5 and 10 GPa by displacing the Ba atoms by 0.1 Å in the Si_{24} cages in the (100) direction which corresponds to the direction towards the center of the hexagons in the Si_{24} chains (see Fig. S5 of the Supplemental Material [54]). It is difficult from our EXAFS signal to conclude that this

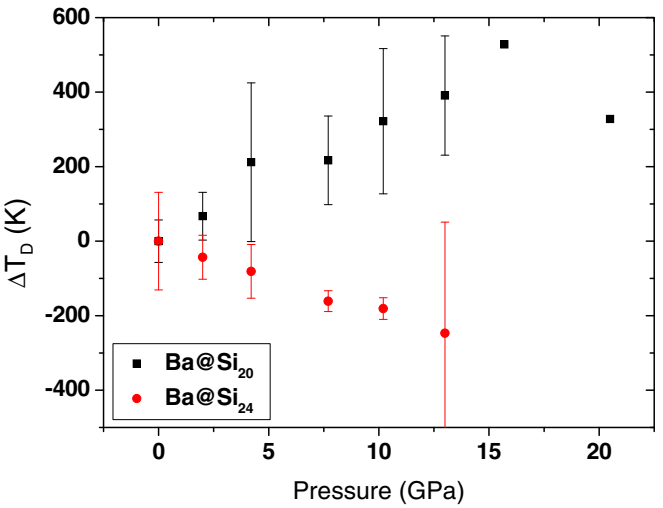

FIG. 8. Relative pressure evolution of the Ba-Si pseudo-Debye temperature in Ba_8Si_{46} in the two different local environments, i.e., the Ba@Si_{20} and Ba@Si_{24} cages.

Ba displacement is what is really taking place as many other hypothesis would need to be verified. In fact, using a higher k domain EXAFS signal, but for pressures below the volume collapse, the main conclusion in Ref. [27] was that the barium atoms remained at the center of the cages up to pressures of 14 GPa, with an incertitude of 0.3 Å. We should note that in Raman studies [26], the presence of a phase transition at 7 GPa was proposed which was attributed to the random displacement of the Ba position inside the Si_{24} cage leading to a cage distortion of the Si host frame and hence a relaxation of the Raman selection rules.

In our experiments, for pressures in the 5–12 GPa range, the Debye temperature associated with the Ba-Si Ba@Si_{24} scattering paths strongly decreases with respect to the one of the Ba@Si_{20} cage. This indicates that from that pressure, there is an important static disorder developing in the Ba@Si_{24} cages. We have to conclude then that there is a progressive static (structural) disorder associated with the Ba-Si scattering paths in the Ba@Si_{24} cage from pressures situated between 5 and 10 GPa.

The EXAFS fits beyond 13 GPa became essentially independent of the model used for the Si_{24} cage, as its contribution to the EXAFS signal appeared as negligible with respect to the one of the Si_{20} cage. Fits became more difficult, with one of the spectra (18.1 GPa) giving larger uncertainties for the pseudo-Debye temperature than the obtained values (we have not then included this point in the graph). The uncertainties of the Ba@Si_{20} pseudo-Debye temperature could not be obtained as shown in Fig. 8. We conclude that for pressures beyond 13 GPa, the local structure model of the low-pressure phase does not apply. This is confirmed by the last point of the Ba@Si_{20} pseudo-Debye temperature in Fig. 8 whose value decreases, which could point to a possible distortion in this cage. In our EXAFS fits, we tried to verify the hypothesis of Iitaka [35] which proposes that the collapse is related to the diffusion of the Si(6c) atoms of the hexagons by fitting occupancy numbers for all the scattering paths involving these

atoms. Unfortunately, the accuracy with which this occupancy number was obtained was insufficient to discriminate this hypothesis. In fact, the Si($6c$) major contribution to the EXAFS signal is related to the Si_{24} cages through the Ba − Si($6c$) scattering paths, but as stated before, after the collapse the contribution of the Si_{24} scattering paths to the EXAFS signal becomes negligible. Examples of EXAFS fits are provided in Fig. S6 of the Supplemental Material [54].

V. DISCUSSION

The EXAFS results show that there is a significant difference between the pressure evolution of the structure and/or dynamics in the two types of cages. The Ba@Si_{20} is the cage keeping the higher spatial/dynamical coherence. The difference between the behavior of the two cages becomes significant from pressures above 5 GPa, which corresponds to the first observed transition of Ba_8Si_{46} at 5–7 GPa [26,27]. The differences between the behavior of the two cages is amplified with pressure up to the volume collapse transition at 10–13 GPa (see Fig. 8). All these changes do not affect the observed pressure evolution of the superconducting T_c (Fig. 5) which progressively decreases down to values of ∼3 K at 14 GPa, in rather good agreement with predictions based on a perfect clathrate crystal [8]. Then, the contribution of the Ba-Si associated phonon modes in the Si_{24} cages to the electron-phonon coupling needs to be discarded. The low energy of the Ba-associated dynamics [6,19] and the importance of the Si sp^3 character on the electron-phonon coupling [8] support the idea that the guest atom dynamics does not participate in the electron-phonon coupling driving the clathrate superconducting character.

At the volume collapse we observe a positive jump of the superconducting critical pressure which increases up to values of ∼8.5–9 K at 20 GPa (Fig. 5) which tends to exclude the possibility of a homothetic volume collapse: a modification of the nanocages' local structure is needed to explain the T_c jump, which could favor in principle either the electron topological transition scenario for the high-pressure phase [30] or the diffusion of some of the silicon atoms [35]. Nevertheless the absence of crystalline silicon diffraction peaks on samples recovered from 17 GPa does not support this last hypothesis. The contribution of the Si_{24} cage to the EXAFS signal vanishes in the high-pressure phase, but it is not possible to establish whether this has been due to a progressive or sudden evolution of the structure or dynamics of the nanocage. Data acquisition in a larger k domain (possible at the Ba K edge) would allow us to apply more advanced EXAFS modeling which coupled with statistical structural simulations [58] should allow us to study eventual local order/disorder effects which could contribute in the high-pressure phase or establish local distortions in the nanocages.

Our work shows that the superconducting character of the clathrate structure can be preserved and even enhanced despite local changes which may affect both the host and the guest structures. This robustness in the superconductivity of the clathrate structure could be related also to the observed superconductivity of $Ag_6O_8AgHF_2$ [59]. In fact, this is the only silver-containing compound in which superconductivity has been observed and its structure is clathrate based.

One of the remaining questions is the possible impact of the Ba vacancies on the observed transition at 5–7 GPa. The very small residual electrical resistance ratio found in our experiments clearly points to a high concentration of defects, which finds as most a possible origin of the Ba deficiency in the Si_{24} cages [43]. In fact, it has been observed in the case of Na-intercalated type-II clathrates an important shift of the Na atoms from the center of the Si_{28} cages [60] which can be interpreted in terms of a Peierls distortion [61] or in terms of particular dynamics [62]. In the case of the type-I structure, the presence of Ba vacancies in certain Si_{24} cages introduces a local symmetry breaking as has also been found in mixed $Ba_8(Si,Ge)_{46}$ clathrates [63]. Such symmetry breaking would affect the Ba-Ba interactions and could be at the origin of the observed incoherence of the EXAFS signal observed in our experiments in the larger cages at pressures beyond 5 GPa when Ba-Ba lattice mediated interactions [19] become more important. XAS and Raman experiments point in fact to a correlation between this lower-pressure transition and Ba displacement from the center of the Si_{24} cages in type-I clathrates. This suggests that this transition could disappear for perfectly stoichiometric Ba_8Si_{46} crystals.

VI. CONCLUSIONS

We have shown that through the Landau theory of a Fermi liquid treatment, the superconducting critical temperature T_c scales with the quadratic term of the resistance dependence with temperature [48]. This allows us to obtain the electron-phonon coupling constant $\lambda = 1.1$ for the low-pressure phase, in very good agreement with published calculations [8]. T_c decreases with pressure monotonically until the volume collapse transition at 10–13 GPa. This evolution is not affected by the strong difference between the local structure evolution with pressure of the two types of nanocages composing the structure Ba@Si_{20} and Ba@Si_{24} which is observed for pressures beyond ∼5 GPa. The evolution of the nanocages' local structure evidences the progression of a structural loss of coherence in the Ba@Si_{24} cages. At pressures above ∼10–13 GPa, corresponding to the volume collapse phase transformation, we observe a sudden increase in the critical temperature with a maximum T_c of ∼8.5–9 K at 20 GPa: the collapsed structure of Ba_8Si_{46} is then superconducting with an enhanced superconductivity. The collapse transition is concomitant with local structure modifications around the Ba atoms evidenced by the near-edge XAS sudden changes. These observations exclude a structural homothecy in the volume collapse transition. The measured superconductivity in the high-pressure collapsed phase of Ba_8Si_{46} points out the robustness of superconductivity in clathrate structures.

[1] H. Kawaji, H.-o. Horie, S. Yamanaka, and M. Ishikawa, Phys. Rev. Lett. **74**, 1427 (1995).

[2] S. Yamanaka, E. Enishi, H. Fukuoka, and M. Yasukawa, Inorg. Chem. **39**, 56 (2000).

[3] A. San-Miguel, P. Keghelian, X. Blase, P. Melinon, A. Perez, J. P. Itie, A. Polian, E. Reny, C. Cros, and M. Pouchard, Phys. Rev. Lett. **83**, 5290 (1999).

[4] X. Blase, P. Gillet, A. San Miguel, and P. Melinon, Phys. Rev. Lett. **92**, 215505 (2004).

[5] G. S. Nolas, J. L. Cohn, G. A. Slack, and S. B. Schujman, Appl. Phys. Lett. **73**, 178 (1998).

[6] S. Pailhès, H. Euchner, V. M. Giordano, R. Debord, A. Assy, S. Gomès, A. Bosak, D. Machon, S. Paschen, and M. de Boissieu, Phys. Rev. Lett. **113**, 025506 (2014).

[7] T. Takabatake, K. Suekuni, T. Nakayama, and E. Kaneshita, Rev. Mod. Phys. **86**, 669 (2014).

[8] D. Connétable, V. Timoshevskii, B. Masenelli, J. Beille, J. Marcus, B. Barbara, A. M. Saitta, G.-M. Rignanese, P. Mélinon, S. Yamanaka, and X. Blase, Phys. Rev. Lett. **91**, 247001 (2003).

[9] H. Wang, J. S. Tse, K. Tanaka, T. Iitaka, and Y. Ma, Proc. Natl. Acad. Sci. **109**, 6463 (2012).

[10] Y. Li, J. Hao, H. Liu, J. S. Tse, Y. Wang, and Y. Ma, Sci. Rep. **5**, 9948 (2015).

[11] S. Bobev and S. C. Sevov, J. Solid State Chem. **153**, 92 (2000).

[12] Edited by G. S. Nolas, *The Physics and Chemistry of Inorganic Clathrates*, Springer Series in Materials Science, Vol. 199 (Springer, Heidelberg, 2015).

[13] J. S. Kasper, P. Hagenmuller, M. Pouchard, and C. Cros, Science **150**, 1713 (1965).

[14] W. Carrillo-Cabrera, S. Budnyk, Y. Prots, and Y. Grin, Z. Anorg. Allg. Chem. **630**, 2267 (2004).

[15] N. Jaussaud, P. Toulemonde, M. Pouchard, A. San Miguel, P. Gravereau, S. Pechev, G. Goglio, and C. Cros, Solid State Sci. **6**, 401 (2004).

[16] H. Fukuoka, J. Kiyoto, and S. Yamanaka, Inorg. Chem. **42**, 2933 (2003).

[17] R. Lortz, R. Viennois, A. Petrovic, Y. Wang, P. Toulemonde, C. Meingast, M. M. Koza, H. Mutka, A. Bossak, and A. San Miguel, Phys. Rev. B **77**, 224507 (2008).

[18] Y. Noat, T. Cren, P. Toulemonde, A. San Miguel, F. Debontridder, V. Dubost, and D. Roditchev, Phys. Rev. B **81**, 104522 (2010).

[19] E. Reny, A. San-Miguel, Y. Guyot, B. Masenelli, P. Melinon, L. Saviot, S. Yamanaka, B. Champagnon, C. Cros, M. Pouchard, M. Borowski, and A. J. Dianoux, Phys. Rev. B **66**, 014532 (2002).

[20] P. Toulemonde, C. Adessi, X. Blase, A. San Miguel, and J. L. Tholence, Phys. Rev. B **71**, 094504 (2005).

[21] R. Viennois, P. Toulemonde, C. Paulsen, and A. San-Miguel, J. Phys.: Condens. Matter **17**, L311 (2005).

[22] K. J. Chang, M. M. Dacorogna, M. L. Cohen, J. M. Mignot, G. Chouteau, and G. Martinez, Phys. Rev. Lett. **54**, 2375 (1985).

[23] E. Bustarret, C. Marcenat, P. Achatz, J. Kacmarcik, F. Levy, A. Huxley, L. Ortega, E. Bourgeois, X. Blase, D. Debarre, and J. Boulmer, Nature (London) **444**, 465 (2006).

[24] A. San-Miguel, P. Mélinon, D. Connétable, X. Blase, F. Tournus, E. Reny, S. Yamanaka, and J. P. Itié, Phys. Rev. B **65**, 054109 (2002).

[25] A. San-Miguel and P. Toulemonde, High Pressure Res. **25**, 159 (2005).

[26] T. Kume, H. Fukuoka, T. Koda, S. Sasaki, H. Shimizu, and S. Yamanaka, Phys. Rev. Lett. **90**, 155503 (2003).

[27] A. San-Miguel, A. Merlen, P. Toulemonde, T. Kume, S. L. Floch, A. Aouizerat, S. Pascarelli, G. Aquilanti, O. Mathon, T. L. Bihan, J.-P. Itié, and S. Yamanaka, Europhys. Lett. **69**, 556 (2005).

[28] L. Yang, Y. M. Ma, T. Iitaka, J. S. Tse, K. Stahl, Y. Ohishi, Y. Wang, R. W. Zhang, J. F. Liu, H.-K. Mao, and J. Z. Jiang, Phys. Rev. B **74**, 245209 (2006).

[29] J. S. Tse, R. Flacau, S. Desgreniers, T. Iitaka, and J. Z. Jiang, Phys. Rev. B **76**, 174109 (2007).

[30] J. S. Tse, L. Yang, S. J. Zhang, C. Q. Jin, C. J. Sahle, C. Sternemann, A. Nyrow, V. Giordano, J. Z. Jiang, S. Yamanaka, S. Desgreniers, and C. A. Tulk, Phys. Rev. B **84**, 184105 (2011).

[31] J. S. Tse, S. Desgreniers, Z.-q. Li, M. R. Ferguson, and Y. Kawazoe, Phys. Rev. Lett. **89**, 195507 (2002).

[32] T. Kume, T. Koda, S. Sasaki, H. Shimizu, and J. S. Tse, Phys. Rev. B **70**, 052101 (2004).

[33] D. Machon, P. Toulemonde, P. F. McMillan, M. Amboage, A. Munoz, P. Rodriguez-Hernandez, and A. San Miguel, Phys. Rev. B **79**, 184101 (2009).

[34] P. Toulemonde, D. Machon, A. San Miguel, and M. Amboage, Phys. Rev. B **83**, 134110 (2011).

[35] T. Iitaka, Phys. Rev. B **75**, 012106 (2007).

[36] T. Kume, T. Fukushima, S. Sasaki, H. Shimizu, H. Fukuoka, and S. Yamanaka, Phys. Status Solidi (b) **244**, 352 (2007).

[37] P. Toulemonde, A. San-Miguel, A. Merlen, R. Viennois, S. L. Floch, C. Adessi, X. Blase, and J. L. Tholence, J. Phys. Chem. Solids **67**, 1117 (2006).

[38] A.-M. Flank, G. Cauchon, P. Lagarde, S. Bac, M. Janousch, R. Wetter, J.-M. Dubuisson, M. Idir, F. Langlois, T. Moreno, and D. Vantelon, Nucl. Instrum. Methods Phys. Res., Sect. B **246**, 269 (2006).

[39] R. A. Forman, G. J. Piermarini, J. D. Barnett, and S. Block, Science **176**, 284 (1972).

[40] A. San-Miguel, Phys. B (Amsterdam, Neth.) **208-209**, 177 (1995).

[41] A. L. Ankudinov, B. Ravel, J. J. Rehr, and S. D. Conradson, Phys. Rev. B **58**, 7565 (1998).

[42] M. Newville, J. Synchrotron Radiat. **8**, 322 (2001).

[43] R. Castillo, W. Schnelle, M. Bobnar, U. Burkhardt, B. Böhme, M. Baitinger, U. Schwarz, and Y. Grin, Z. Anorg. Allg. Chem. **641**, 206 (2015).

[44] M. Kaveh and N. Wiser, Adv. Phys. **33**, 257 (1984).

[45] M. Gurvitch, Phys. Rev. Lett. **56**, 647 (1986).

[46] N. G. Ptitsina, G. M. Chulkova, K. S. Il'in, A. V. Sergeev, F. S. Pochinkov, E. M. Gershenzon, and M. E. Gershenson, Phys. Rev. B **56**, 10089 (1997).

[47] G. Garbarino and M. Nunez-Regueiro, Solid State Commun. **142**, 306 (2007).

[48] M. Nunez-Regueiro, G. Garbarino, and M. D. Nunez-Regueiro, J. Phys.: Conf. Ser. **400**, 022085 (2012).

[49] G. Morard, M. Mezouar, N. Rey, R. Poloni, A. Merlen, S. Le Floch, P. Toulemonde, S. Pascarelli, A. San-Miguel, C. Sanloup, and G. Fiquet, High Press. Res. **27**, 223 (2007).

[50] J. Z. Hu, L. D. Merkle, C. S. Menoni, and I. L. Spain, Phys. Rev. B **34**, 4679 (1986).

[51] J. P. Itié, A. Polian, D. Martinez, V. Briois, A. Di Cicco, A. Filipponi, and A. SanMiguel, J. Phys. IV France **7**, C2 (1997).

[52] J. J. Rehr and R. C. Albers, Rev. Mod. Phys. **72**, 621 (2000).

[53] A. Filipponi, A. Di Cicco, and C. R. Natoli, Phys. Rev. B **52**, 15122 (1995).

[54] See Supplemental Material at http://link.aps.org/supplemental/10.1103/PhysRevB.94.104507 for more details on the XAS data and its analysis.

[55] V. Briois, C. Brouder, P. Sainctavit, A. San Miguel, J.-P. Itié, and A. Polian, Phys. Rev. B **56**, 5866 (1997).
[56] J. Pellicer-Porres, A. San Miguel, and A. Fontaine, J. Synchrotron Radiat. **5**, 1250 (1998).
[57] P. Fornasini and R. Grisenti, J. Synchrotron Radiat. **22**, 1242 (2015).
[58] G. Ferlat, J.-C. Soetens, A. S. Miguel, and P. A. Bopp, J. Phys.: Condens. Matter **17**, S145 (2005).
[59] K. Kawashima, M. Kriener, M. Ishii, Y. Maeno, and J. Akimitsu, Phys. C (Amsterdam, Neth.) **468**, 464 (2008).
[60] F. Brunet, P. Melinon, A. San Miguel, P. Keghelian, A. Perez, A. M. Flank, E. Reny, C. Cros, and M. Pouchard, Phys. Rev. B **61**, 16550 (2000).
[61] H. Libotte, J. Gaspard, A. San Miguel, and P. Melinon, Europhys. Lett. **64**, 757 (2003).
[62] M. Beekman, W. Schnelle, H. Borrmann, M. Baitinger, Y. Grin, and G. S. Nolas, Phys. Rev. Lett. **104**, 018301 (2010).
[63] J.-C. Blancon, D. Machon, V. Pischedda, R. Debord, P. Toulemonde, S. Le Floch, S. Pascarelli, P. Mélinon, and A. San-Miguel, Phys. Rev. B **93**, 134103 (2016).